Low-cloud fraction, lower-tropospheric stability and large-scale divergence

YUNYAN ZHANG[1,2]*, BJORN STEVENS[1,3], BRIAN MEDEIROS[1], MICHAEL GHIL[1,4]

[1]Department of Atmospheric and Oceanic Sciences

University of California at Los Angeles, Los Angeles, California

[2]Lawrence Livermore National Laboratory, Livermore, California

[3]Max Planck Institute for Meteorology, Hamburg, Germany

[4]Geosciences Department and Laboratoire de Météorologie Dynamique de CNRS/IPSL,

Ecole Normale Supérieure, Paris, France

To be submitted to Journal of Climate

*Corresponding author: Lawrence Livermore National Laboratory, Mail Code L-103, P.O. Box 808, Livermore, CA 94551 Email: zhang25@llnl.gov

ABSTRACT

This paper explores the capability of the mixed-layer model (MLM) to represent the observed relationship between low-cloud fraction and lower-tropospheric stability; it also investigates the influence of large-scale meteorological fields and their variabilities on this relationship. The MLM's local equilibrium solutions are examined subject to realistic boundary forcings that are derived from reanalysis data of European Center for Medium Range Weather Forecasts (ERA-40). The MLM is successful in reproducing the positive correlation between low-cloud fraction and lower-tropospheric stability. The most accurate relationship emerges when the forcings capture synoptic variability, in particular the daily varying large-scale divergence is a leading factor in improving the regression slope.

The feature of the results is mainly attributed to the model cloud fraction's intrinsic nonlinear response to the divergence field. Given this nonlinearity, the full range of divergence must be accounted for, since a broad distribution of divergences will give a better cloud fraction overall, although model biases might still affect individual MLM results. The model cloud fraction responds rather linearly to lower-tropospheric stability; and the distribution of the latter is less sensitive to sampling at different timescales than divergence. The strongest relationship between cloud fraction and stability emerges in the range of intermediate stability values. This conditional dependence is evident in both model results and observations. The observed correlation between cloud fraction and stability may thus depend on the underlying distribution of weather noise, and hence may not be appropriate in situations where such statistics can be expected to change.

1. Introduction

Low-level stratiform clouds have long been recognized as essential to Earth's radiative balance. Their parametric representation in large-scale models, such as global climate models (GCMs) and numerical weather prediction models, has proved challenging; in part due to the difficulty of representing the structure of the environment in which they are found, and the processes operating therein. The main challenge proves to be an accurate representation of the temperature inversion that caps these cloud layers, thereby limiting mixing with the free troposphere, which in turn allows moisture to accumulate within the marine boundary layer and clouds to form.

Empirically motivated parameterizations have long attempted to take advantage of the relationship between low-cloud fraction (or amount) and the strength of the temperature inversion, so as to better represent these clouds. For instance, Slingo (1987) proposed diagnosing low-cloud fraction (LCF) from the strength of the modeled temperature inversion. Klein and Hartmann (1993) (hereafter KH93) showed that the lower-tropospheric stability (LTS), which they defined as the potential temperature difference between surface and 700 hPa, provides a remarkable indicator of low-cloud fraction on seasonal timescales. Their result is reproduced in Figure 1 and shows their linear regression between seasonal area mean LTS and LCF for the six subtropical stratocumulus regions identified in Figure 2. Also shown is a modern reconstruction of this relationship using different data sources. This remarkable association has begun to be used as the basis for parameterizations of low clouds in some large-scale models (*e.g.*, Collins et al. 2004). Some reasons why this might not be a good idea are that: (i) the association breaks down on shorter time-scales (Klein and Hartmann 1993; Klein et al. 1995; Klein 1997); (ii) because lower-tropospheric stability is dimensional, to the extent the relation expresses a climate truth, this truth may well depend on the climate state; (iii) the association varies regionally (Stevens et al. 2007). A more attractive solution would be a theory, or physically based model, that when integrated in a global climate model, yielded the observed association between low-cloud fraction and lower-tropospheric stability. Such a theory would have the benefit of helping understand what underlies this correlation.

For decades, our understanding of the stratocumulus-topped boundary layer (STBL) has been rooted in the mixed-layer theory of Lilly (1968), and it seems likely that any parameterization will incorporate important elements of these ideas. Some groups (Suarez et al. 1983; Randall et al. 1985; Moeng and Stevens 1999; Medeiros et al. 2005) have attempted to implement Lilly's ideas directly, by introducing the mixed-layer model (MLM) directly as a GCM parameterization. Others have been experimenting with approaches which relax to the MLM in certain limits (Lock 2001; Grenier and Bretherton 2001). Because the mixed-layer concept dominates our thinking about how to parameterize stratocumulus, off-line studies have explored the capability of the MLM to represent the STBL. For instance, Stevens (2002) used such a model to evaluate a variety of proposed entrainment parameterizations. With weak entrainment rates, the MLM is able to simulate a reasonable diurnal evolution of well-mixed STBL (Zhang et al. 2005) and is characterized by equilibrium states comparable to observations (Stevens et al. 2005). Bretherton and Wyant (1997) further showed that a MLM can be used to evaluate the point at which the cloud layer "decouples" (thermodynamically differentiates itself) from the sub-cloud layer, thereby invalidating the underlying assumptions in the model. However it still remains a question whether the MLM is able to reproduce the observed relationship between low-cloud fraction and lower-tropospheric stability; and if so, what meteorological parameters and variabilities make the representation of the observed relationship more precisely?

In this study, we endeavor to answer these questions by exploring local equilibrium solutions of a MLM subject to realistic boundary forcings derived globally from the European Center for Medium Range Weather Forecasts (ECMWF) Reanalysis (ERA-40, Uppala *et al.* 2005) averaged over a variety of timescales.

The choice of local equilibrium solutions, wherein advective tendencies are prescribed independently of the solution at neighboring points, is motivated by practical and theoretical considerations. From a practical perspective, equilibrium solutions are much easier to obtain, in part because they no longer depend on solutions at neighboring grid points. This proves necessary as there are circumstances where a mixed-layer solution may not be a good representation of the boundary layer, and so removing the dependence of solutions on one point from solutions at other points avoids the problem associated with unphysical solutions within the domain. From a theoretical perspective the equilibrium solutions are attractive as they remove time as a variable, and thus facilitate attempts to relate the statistics of the model to the statistics of the underlying forcing.

The disadvantage of focusing on equilibrium solutions is that they are not a realistic representation of the expected state of the boundary layer. Such solutions would only be expected to be physically representative in the limit when the adjustment timescale of the boundary layer is much shorter than the timescale over which the forcing changes. Schubert et al. (1979) showed that the adjustment time scale to MLM equilibrium is about one week for boundary layer depth and one day for thermodynamic fields, which implies that the history is important to any particular realization of the boundary layer state. Even so, one could imagine that the equilibrium of the MLM is at least a good indicator of the expected state of any particular realization, *i.e.,* cloud equilibria are likely to be cloudy, and cloud-free equilibria are likely to be cloud free, especially when the model forcing time scale is long, such as seasonal or monthly mean. This motivates our working hypothesis, which is that the statistics of the MLM equilibria capture essential aspects of the actual boundary layer. Given this distinction, we note that the failure of the MLM to reproduce the observed climatological relationships may just as well stem from the failure of our equilibrium hypothesis as from an intrinsic shortcoming of the MLM.

We organize the remainder of this paper as follows: the methodology employed is presented in section 2, including a discussion of our implementation of the MLM, its boundary conditions and the set-up of simulations, as well as the data sources used to force and evaluate it. The equilibrium climatology of low-cloud fraction is presented and interpreted in section 3; section 4 provides a framework for discussing our findings in relation to observations; a summary and conclusions appear in section 5.

2. Methods

a. Data

The meteorological state used in our calculations and data-analysis is derived almost entirely from the ERA-40 6-hourly data. Previous work has shown this analysis to provide an adequate representation of the remote marine boundary layer, at least in the stratocumulus region west-southwest of California (Stevens et al. 2007). Based on ERA-40 sea surface temperature (SST), pressure and 10 m winds, we calculate the large-scale divergence, $\mathcal{D}$, surface wind speed, $\|U\|$, and surface values of the liquid-water static energy and total water specific humidity, which we denote by $s_{l,0}$ and $q_{t,0}$, respectively. While the MLM is most suitable for marine stratocumulus boundary layers, we also include the Chinese stratus region, where most of the domain is over land, to maintain consistency with KH93. In the Chinese stratus region, surface air temperature is used instead of SST.

Cloud fraction is taken from the International Satellite Cloud Climatology Project (ISCCP, Rossow and Schiffer 1999). In our analysis the correlation between low-cloud fraction and lower-tropospheric stability is not as strong and the slope of the regression is somewhat weaker (5% cloud fraction per degree Kelvin in our case as compared to 6% per degree Kelvin) than reported by KH93. Differences may have a number of origins: (i) low-cloud fraction is measured differently by ISCCP than it was by KH93, who used the cloud climatology derived from the surface observer network; (ii) the ISCCP low-cloud fraction is taken as the sum of stratocumulus and stratus cloud fraction below 680 hPa, in which no cloud overlap is considered; (iii) we use a different source of data for estimates of the lower-tropospheric stability; (iv) we are exploring a slightly different epoch (or temporal period). In the following we evaluate the MLM results with the ISCCP regression line, with the knowledge that the true low-cloud climatology exhibits some quantitative dependence on the data source. Finally, we note that although Wood and Bretherton (2006) show that seasonal means of reconstructed (or estimated) inversion stability more strongly correlate with low-cloud fraction than lower-tropospheric stability, this largely arises from improved behavior in the extra-tropics. Because our study focuses almost exclusively on the subtropical stratocumulus regions (as shown in Figure 2), where such reconstructions have less effect and because we began before we became aware of their results, we maintain our emphasis on the traditional definition of lower-tropospheric stability.

b. The MLM

The structure of well-mixed stratocumulus-topped boundary layer is illustrated in Figure 3 from Stevens et al. (2007). The MLM consists of three prognostic equations for mass (h, the height of the stratocumulus-topped boundary layer, also the cloud top height), liquid water moist static energy ($s_l = c_p T + gz - L_v q_l$), and the total moisture ($q_t = q_v + q_l$, the sum of waver vapor and liquid water specific humidity). Both s_l and q_t are adiabatic invariants of the system. In the following, $\langle \mathcal{X} \rangle = \frac{1}{h}\int_0^h \mathcal{X} dz$, stands for the vertically averaged, or bulk value, and $\mathcal{X} \in \{s_l, q_t, \tilde{u}\}$, where $\tilde{u}$ is the horizontal wind vector. The equations we wish to solve are as follows:

$$\frac{dh}{dt} = E - \mathcal{D}h - \langle \tilde{u} \rangle \cdot \nabla h \tag{1}$$

$$\frac{d}{dt}\langle s_l \rangle = \frac{1}{h}[V(s_{l,0} - \langle s_l \rangle) + E(s_{l,+} - \langle s_l \rangle) - \triangle F_R] - \langle \tilde{u} \rangle \cdot \nabla \langle s_l \rangle \tag{2}$$

$$\frac{d}{dt}\langle q_t \rangle = \frac{1}{h}[V(q_{t,0} - \langle q_t \rangle) + E(q_{t,+} - \langle q_t \rangle)] - \langle \tilde{u} \rangle \cdot \nabla \langle q_t \rangle \tag{3}$$

The evolution of the cloud top height, h, is represented as a balance between the entrainment velocity E, downwelling large-scale flow $\mathcal{D}h$ (which we scale with the surface divergence), and large-scale advection. The evolution of s_l is affected by surface fluxes, entrainment, the cloud-top radiative flux divergence $\triangle F_R$, and advection. In the absence of precipitation, the evolution of q_t is determined by surface fluxes, entrainment and advection. Subscript 0 and + denote surface values and the states just above cloud top respectively. Surface fluxes are calculated by a bulk aerodynamic formula, where $V = C_D \|U\|$, with $\|U\|$ the surface wind speed, and C_D the surface exchange coefficient, which is assumed constant. Here, $\Delta F_R = f_p(1 - e^{-\kappa L})$. The cloud liquid-water path, L, is diagnosed based on $h,\ s_l$ and q_t, while κ is an empirical coefficient equal to 85 m^2 kg^{-1} (Stevens et al. 2003b) and $f_p = 40$ Wm^{-2} is chosen to represent a diurnally averaged value of this quantity, and is loosely based on observations during The Second Dynamics and Chemistry of Marine Stratocumulus field study (DYCOMS-II Stevens et al. 2003a).

To close Eqs. (1)–(3) requires the specification E. We use a composite formula which incorporates both buoyancy and wind-shear. For the buoyancy component, the scheme from Lewellen and Lewellen (1998) is adopted with the entrainment efficiency $\eta = 0.25$ (Stevens et al. 2003b). The wind-shear component is assumed proportional to an e-folding profile as follows:

$$E_w = C_w e^{-z/500} \tag{4}$$

where z is the height; C_w = 0.61 mm s^{-1}, is an empirical constant.

Allowing both processes to contribute to entrainment yields multiple-equilibria shown in Figure 4. For a certain range of large-scale conditions, such as $\mathcal{D}$, the MLM has two stable solutions, cloudy and clear sky, in which the final states are determined by the position of the initial state relative to the unstable solution (Randall and Suarez 1984; Stevens et al. 2005). An example is shown in Figure 5. The cloud fraction is reduced about 13 % averaged over the California stratocumulus region when initial conditions are changed from cloudy to clear-sky states. Because in the stratocumulus regions we are familiar with, alongshore flow is more common than offshore flow, in our study, all the calculations are initiated from cloudy states.

c. Implementation

1) Large-scale boundary conditions

Most of the boundary conditions and forcings are straightforward to apply. Exceptions include the advection terms, and the specification of $s_{l,+}$. In lieu of calculating advection directly (which would require knowledge of the solution at the upwind grid point), we advect the surface properties of the upwind grid–points into the domain, and surface properties of the local grid out of the domain. That is, thermodynamic gradients within the boundary layer are assumed to follow gradients in surface properties. This assumption is good in the limit of weak entrainment, but is more problematic in situations where entrainment fluxes are more substantial and we anyway do not expect stratocumulus. Mass advection, as represented by the $\langle \tilde{u} \rangle \cdot \nabla h$ term, is modeled through the use of the ERA-40 boundary layer height. The absolute value of h is significantly underestimated by the ERA-40 representation of the stratocumulus region of the north-east subtropical Pacific, however such underestimation is distributed consistently, thus ∇h appears reasonable in the climatology and motivates the model used here (*cf. Stevens et al. 2007)*.

The inversion strength at the top of cloud depends in part on $s_{l,+}$. Because of the long-wave radiation flux divergence, the air cools just above the cloud top. Due to this fine-scale process, a linear extrapolation based on the upper troposphere temperature and the lapse rate overestimates the temperature by 2-5 K at the cloud top (Siems et al. 1993; Stevens et al. 2003b; Caldwell and Bretherton 2008). Therefore, a 4 K offset is added to the linear extrapolation in order to capture the curvature of θ_l at the bottom of the inversion just above the cloud top shown in Figure 3. Some sensitivity to this offset is evident in the solutions; 4 K appears to be a reasonable value based on previous modeling and simulation work.

2) Solution method

Solving for the equilibria of the model is not trivial. Although analytic solutions exist for some simple models of the entrainment velocity, we were not able to derive solutions given our representation of entrainment. Hence we look for equilibria by integrating the model in time. Integrations are conducted for 200 days, and convergent solutions are identified as those which do not change by more than 0.01% over thirty minutes. We only seek solutions for values for $\mathcal{D} > \mathcal{D}_c = 0.5 \times 10^{-6}\ \mathrm{s}^{-1}$; $\mathcal{D}_c$ is a critical value for divergence; its sole purpose is to help limit the domain over which solutions are sought and thus minimize the computational expense. Even so, for weak stability and values of $\mathcal{D}$ near $\mathcal{D}_c$ the model equilibria can be unphysically deep. Thus we further set a threshold depth of $z_c = 2000\, m$, so that equilibria with $h > z_c$ are discarded. Regions without acceptable equilibria are assigned a missing value, and are assumed to be cloud free. In reality they may be cumulus capped, but given the generally small value of cumulus cloud cover (*e.g.*, about 10%, Siebesma et al. 2003), and (more importantly) the fact that cumulus clouds are not intended to contribute to the ISCCP low-cloud fraction as defined here, such an assumption appears appropriate.

It would be more reasonable to use physical criteria such as the buoyancy-flux integral ratio to determine decoupling (Turton and Nicholls 1987; Bretherton and Wyant 1997; Wyant et al. 1997; Stevens 2000). To estimate this, we used a similar diagnostic parameter, radiative entrainment efficiency α, as a measure of decoupling. Previous work (Zhang et al. 2005) suggests α represents the contribution to turbulence kinetic energy generation from surface fluxes and radiative driving; $\alpha > 1$ leads to decoupling. However this criteria did not discriminate well the MLM equilibria, we think the reasons are that: i) the common decoupling mechanisms such as diurnal varying radiative driving or drizzling are not included; ii) the transition might be more evident in transient evolution with continuously time-varying boundary conditions and hence sensitive to initial data. This certainly requires further research by improving the sophistication of the model. Possible approaches would be to investigate the low-cloud climatology by the Lagrangian integration along the backward trajectory starting with realistic initial conditions (Bretherton and Wyant 1997) or to use predictor-corrector schemes to calculate large-scale advection tendencies based on ERA-40 data and MLM simulations. Such approaches might also improve liquid water path, which is largely overestimated in equilibrium states.

Clearly a number of these choices are not ideal, and while physically motivated, they introduce a number of arbitrary parameters. We have attempted to insure that our findings do not depend essentially on these choices, and recognize the limitations of our study, many of which stem from the lack of a compelling theory or unified model of cloud-topped boundary layers, as this prohibits us from exploring non-equilibrium solutions as continuous functions of space and time.

3) Solution Domain

The MLM simulation domain is a gaussian grid with a spacing of about 1.5° by 1.5°. This corresponds to the NCAR Data Support Section refined T85 grid, on which the ERA-40 products used here have been regridded. Solutions are sought at a variety of timescales ranging from timescales of daily (1 day) to seasonal (90 days). Integrations are performed using 12 years of data (1990 – 2001), yielding 12 independent estimates of climatological cloud fraction for a seasonal run and about 1080 calculations for the daily run per grid–point per season. The low-cloud fraction is diagnosed as 1 or 0 based on equilibrium cloud liquid water path for each estimate, hence cloud fraction only emerges by averaging over the ensemble of solutions. Further, because most of our focus is on the roughly 50 ERA-40 grid–points in each of the six subtropical stratiform regions in Figure 2, our sample space increases accordingly.

We define a "control run" as one in which all the large-scale boundary conditions are averaged and used to force the MLM at the same timescale. A "sensitivity run" is defined to be set of calculations in which large-scale boundary conditions are averaged and used to force the MLM at different timescales, *e.g.* daily-varying lower-tropospheric stability is used to force the MLM while other boundary conditions are fixed at their seasonal mean value. Unless otherwise stated, simulations should be understood to be "control" runs.

3. MLM Equilibrium Low-Cloud

a. The seasonal cycle of low-cloud fraction

The MLM climatology of seasonal low-cloud fraction compares favorably with the ISCCP observations. This is true for solutions forced with both seasonal and daily varying data, although the latter compare more favorably with the observations. This is evident in Figure 6, in which the seasonal climatology produced from the daily runs follows the seasonal climatology from ISCCP more closely than the climatology from the seasonal runs. The seasonal climatology of daily runs is deficient in some regions and some seasons, most markedly in the Atlantic, where the Namibian stratocumulus region shows the most pronounced differences between what is modeled and observed.

The equilibria of the MLM also credibly differentiate the stratocumulus regions from regions where other cloud regimes prevail. This is evident on maps of seasonal mean low-cloud fraction, as shown in Figure 7.

A more statistical view, which better corresponds to Figure 1 is presented in Figure 8. Again both seasonally and daily forced runs credibly represent the climatology; although the regression slope from the runs forced by daily data is in better accord with the observations. It is noteworthy that the results based on the seasonal forcing are more regionally distinct than those based on daily forcing, with different regions evincing more distinct relationships between low-cloud fraction and lower-tropospheric stability. This suggests that the large magnitude of regression in the seasonally forced climatology comes from differences among regions rather than seasons. For instance, low-cloud fraction for all the seasons in California and Namibia are above the regression line while the low-cloud fraction from Peru and China are all below the regression line. Individual points from climatologies derived from daily forcing are more evenly distributed along the regression line.

These findings suggest that: (i) the positive correlation between low-cloud fraction and lower-tropospheric stability is well reproduced by equilibria of the MLM; and (ii) when subject to daily variations in the ERA-40 boundary conditions, the regression slope is more consistent with data.

Because the relationship between low-cloud fraction and lower-tropospheric stability is not dimensionally consistent, there exists the possibility that the empirical correlation evident between the two quantities is mediated by a dimensional variable that may vary with changing climatological conditions. Exploring such relationships using the MLM allows us to explore the space of its solutions in terms of appropriate non-dimensional representations of the model, the details of which are presented in an appendix. It comes as little surprise that our main finding is that the simple variable[1] that captures the most variance over the stratocumulus regions is the stability

[1]Although we have yet to find one, it remains possible that a combination of the non-dimensional variables we

across the stratocumulus-topped boundary layer normalized by the surface temperature, and the correlation of this variable with low-cloud fraction is commensurate with the correlation between low-cloud fraction and lower-tropospheric stability.

b. Contributions to the simulated climatology of low-cloud fraction

Here we attempt to understand what aspects of the forcing contribute most to the improvement in the representation of the low cloud climatology as one progressively includes finer temporal scales. We explore this question by first asking how much variability in the forcing is necessary for the MLM to capture the observed climatology, and then systematically compare sensitivity runs constructed using seasonally–varying forcing in all but one field, for which daily–varying forcing is applied.

The general behavior of the climatology improves systematically as higher frequency forcing is included, through periods of about three days. This finding is illustrated in Figure 9, showing the regression slope and correlation coefficients between low-cloud fraction and lower-tropospheric stability for runs forced at increasingly higher frequencies. Although the regression slope between low-cloud fraction and lower-tropospheric stability for runs forced on daily timescales looks more like our analysis of the observations (*i.e.,* the point labeled ISCCP in the figure), the difference is not large relative to the uncertainty in the observed relationship (*i.e.,* between ISCCP and KH93). Moreover, the correlation coefficient does not improve relative to runs forced with three-day averaged data.

In Figure 9, sensitivity tests also show that among the variety of forcings (LTS, surface temperature, free troposphere temperature and humidity, advections, divergence), those which contribute directly to the evolution of the mass field (subsidence as represented by daily variations in divergence, and advection of boundary layer depth) are more important to a good representation of the

identify in the appendix captures the variance in the solutions somewhat better than the normalized stability across the stratocumulus-topped boundary layer.

low-cloud climatology.

The extent of variability of the divergence on daily timescales is large. Figure 10 shows the pattern of $\mathcal{D}$ on seasonal and daily timescales. The familiar pattern of subtropical divergence focused over eastern boundary currents is apparent in the seasonal average, but not on daily timescales. This reminds us that the weather noise is as strong as the spatial variability, and that coherent patterns of $\mathcal{D}$ only emerge on longer timescales. Such synoptic variability effectively broadens the probability distribution of divergence, incorporating such variability within the MLM helps it sample a broader state space as it builds up the low-cloud climatology.

Similar benefits are not as apparent when the thermodynamic forcing incorporates variability from shorter timescales. For instance, lower-tropospheric stability is shown in Figure 11. Here the decorrelation between the patterns averaged over short- and long-time periods is less evident than it was for the divergence. Yet it is precisely the stability of the lower troposphere which correlates uncannily with low-cloud fraction in the observational data. Why do the equilibria of the MLM reproduce the observed correlations between low-cloud fraction and lower-tropospheric stability and improve most when the synoptic variability of $\mathcal{D}$ is incorporated?

Part of the answer is that the full distribution of thermodynamic variables is relatively better sampled by the seasonal variability than the divergence. This point is made by Figure 12 and 13 which show the standard deviation of daily mean and seasonal mean data relative to the long-term seasonal area-means. For example, in June, July and August at California region, the ratio of standard deviations between daily and seasonal data is about 0.7 for lower-tropospheric stability while only 0.3 for divergence. In general this ratio is higher for stability than divergence, however there are exceptions: two seasons in Peru and one season in Namibia. Long-term divergence value is approximately between 2.5 to 4×10^{-6} s^{-1} and the daily standard deviation could be as large as 4×10^{-6} s^{-1}.

Figure 14 presents the expected behavior of the MLM for the sub-ensemble consisting of grid–points in stratocumulus regions whose seasonal area-mean values of divergence fall between 2.5 to 4×10^{-6} s^{-1} and whose lower-tropospheric stability is between 16 to 22 K , ranges in which most long-term seasonal area-means are found (*cf.* Figure 12 and 13). The seasonal variance of divergence is significantly less than the variance apparent on daily timescales, thereby further quantifying what we inferred previously.

On average, cloud fraction increases nonlinearly as a function of divergence, hence the width of the distribution matters. This point is also made in Figure 14, whose interpretation benefits from the introduction of some notation. Let $\mathcal{D}_s$ denote the seasonal area-mean value of $\mathcal{D}$ for a sub-ensemble of grid points, and x_ϕ the state vector exclusive of ϕ, so (for instance) $x_\mathcal{D}$ represents all the state variables except divergence. Then the conditional cloud fraction is

$$\overline{c}(\mathcal{D};\mathcal{D}_s) = \int_{-\infty}^{\infty} c(\mathcal{D}, x_\mathcal{D};\mathcal{D}_s)\,\mathrm{d}x_\mathcal{D}, \tag{5}$$

which is plotted as the light solid line in the top panel of Figure 14. The conditional cumulative distribution follows as $\int_{-\infty}^{\mathcal{D}} \overline{c}(\mathcal{D}';\mathcal{D}_s)\,\mathrm{d}\mathcal{D}'$ and is shown as the dark solid line in the figure. The dashed lines show $p(\mathcal{D};\mathcal{D}_s)$, the probability density function of $\mathcal{D}$ conditioned on $\mathcal{D}_s$, both for the daily (dark) and seasonal (light) data. The lower panel in Figure 14 shows analogous quantities but now retaining the lower-tropospheric stability as the random variable.

Generally the MLM produces more cloud with increasing divergence, at least until a point, after which the increasing probability of solutions consisting of shallow, but cloud-free, boundary layers becomes apparent. Because the breadth of the distribution of $\mathcal{D}$ is large as compared to the response of the model, $\overline{c}(\mathcal{D})$ is a non-linear function of $\mathcal{D}$ over a representative range of $\mathcal{D}$. The same is not true for lower-tropospheric stability (LTS, also denoted by Δs_l in the following). The distribution of LTS is quite similar when sampled at daily versus seasonal timescales. Moreover, across the range of observed Δs_l, $\overline{c}(\Delta s_l;\mathcal{D}_s)$ varies more or less linearly. This means that: (i) estimates of $\overline{c}$ which do not sample the full distribution of $\mathcal{D}$ will be biased; and (ii) estimates of $\overline{c}$ are likely to be less sensitive to the distribution of Δs_l, both because the distribution broadens less at small timescales, and because over the range of Δs_l, $\overline{c}(\Delta s_l;\mathcal{D}_s)$ is effectively linear.

Because $\overline{c}(\mathcal{D})$ is non-linear, the breadth of the distribution also insulates against model biases. To appreciate this point, approximate the probability density function of $\mathcal{D}$ as normally distributed about its seasonal value such that

$$p(\mathcal{D}) = \frac{1}{\sigma\sqrt{2\pi}} e^{-(\mathcal{D}-\mathcal{D}_s)^2/(2\sigma^2)}, \quad \mathcal{D} \in (-\infty, \infty) \tag{6}$$

and suppose that the conditional cloud fraction can be written as a Heaviside function, such that

$$\overline{c}(\mathcal{D}) = \begin{cases} 0, & \mathcal{D} < \mathcal{D}_c \\ 1, & \mathcal{D} \geq \mathcal{D}_c \end{cases}, \tag{7}$$

then it is a straightforward matter of integration to show that the expected value of the cloud fraction, C takes the form

$$C = \int_{-\infty}^{\infty} \overline{c}(\mathcal{D})\, p(\mathcal{D})\, \mathrm{d}\mathcal{D} = \frac{1}{2}\left[1 - \mathbf{erf}\left(\frac{\mathcal{D}_c - \mathcal{D}_s}{\sigma\sqrt{2}}\right)\right]. \tag{8}$$

This shows that in the case when $\mathcal{D}_s \approx \mathcal{D}_c$ biases in the cloud model (for instance as represented by biases in $\mathcal{D}_c$) are amplified if the variance in $\mathcal{D}$ is undersampled. Thus including the full breadth of the distribution of $\mathcal{D}$ in our estimates may lead to a better correspondence with the data for the simple reason that it reduces the sensitivity of the results to biases in the model (which in terms of the above arguments could be construed as errors in the modeled value of $\mathcal{D}_c$).

c. On the emergence of low-cloud fraction and lower-tropospheric stability relationships

Figure 14 also helps explain why correlations between low-cloud fraction and lower-tropospheric stability are more evident than, say, correlations between low-cloud fraction and divergence. In effect it says that for a sub-ensemble constructed for grid–points with seasonal area-mean values of $\mathcal{D}$ falling within a narrow range, the cloud fraction, $\overline{c}(\Delta s_l)$, varies roughly linearly with lower-tropospheric stability, Δs_l; given a value of Δs_l over the range of Δs_l in the sub-ensemble, the confluence of other factors is more likely to produce cloud equilibria of the MLM at larger values of Δs_l as opposed to smaller values. The same is not true for divergence. Because individual solutions of the MLM are either zero or one, the slope of $\overline{c}(\Delta s_l)$ in the lower panel of Figure 14, reflects the underlying distribution of $x_{\Delta s_l}$, *i.e.,* components of the state vector exclusive of Δs_l.

Because there is no reason to suspect these distributions to be universal, one should not expect $\mathrm{d}\bar{c}(\Delta s_l)/\mathrm{d}\Delta s_l$ to be universal.

This raises the question as to whether the correlation between lower-tropospheric stability and cloud fraction that is so evident in the data is also valid locally, or only emerges through a composition of data from different regions. This question is interesting to ask of the MLM, even if we know such relationships do not hold in the data, because by evaluating its equilibria we mitigate against the effects of weather noise. To provide an answer we calculate $\mathrm{d}\bar{c}(\Delta s_l)/\mathrm{d}\Delta s_l$ for each region and each season, and plot the local slope along with the global regression in Figure 15. For the most part the local slopes follow the global regression, especially for intermediate values of lower-tropospheric stability. Although in each case it must be emphasized that the correlation underlying these local relationships may not be large, there does tend to be a robustness to such relationships more locally.

The tendency of the local slopes to be flatter at the more extreme values of lower-tropospheric stability is not unlike what we see in Figure 14 for the sub-ensemble based on grid–points with similar values of $\mathcal{D}_s$. To the extent that the equilibria of the MLM capture the essence of real stratocumulus, one could infer from this exercise that: (i) the failure of individual stratocumulus regions to show a robust correlation between low-cloud fraction and lower-tropospheric stability on shorter temporal scales reflects the effect of weather noise; (ii) and while the relationships may be valid given sufficiently restricted conditions, parameterizations based on observed correlations emerging on seasonal timescales are not likely to be valid outside of this range—for instance away from well identified stratocumulus regions, or across changing climate regimes.

4. On the generality of low-cloud fraction and lower-tropospheric stability relationships

To expand on these ideas from the mixed-layer model we return to the observational data and ask: (i) within stratocumulus regimes how robust is the data to our choice of sub-ensemble to composite? (ii) to what extent does the relationship between low-cloud fraction and lower-tropospheric stability depend on one's choice of regime?

The first question is explored by looking at the distribution of the slopes of the regression lines derived by random sampling of seasonal means in the set of points (location and year) comprising four of the stratocumulus regions (Australia, Peru, Californian and Namibian). Our choice to only draw samples from these four regions was motivated by the fact that climatologically these regimes appear most similar and Canarian region is not included because its lower-tropospheric stability is relatively lower than others (*cf.* Figure 13). The distribution of regression slopes from the MLM is similar to that for the data, although markedly weaker (Figure 16), perhaps reflecting the poor behavior of the MLM equilibria over the Namibian region.

This result hints that the relationship between low-cloud fraction and lower-tropospheric stability depends on how different regimes are sampled. This point emerges more clearly when we expand upon this strategy, constructing the distribution of regression slopes by randomly selecting points from regions favoring marine stratocumulus. Here we define a stratocumulus point as maritime regions satisfying: lower-tropospheric stability ≥ 18.55 K, $\omega_{500} \geq 10$ hPa/day, and $\omega_{700} \geq 10$ hPa/day in at least one season of a particular year, where ω_p is the seasonally averaged vertical velocity at some pressure level, p, which measure in hPa. Points satisfying these criteria in their climatological annual cycle are shown by the gray scale in Figure 2. Figure 16 shows that the distribution of regression slopes is somewhat narrower and slightly stronger than when the four geographical stratocumulus regions above are used as the only constraint. This relatively narrow distribution reflects the strength of the criteria used, which select points with similar conditions, and probably a very narrow range of seasonal average divergence, allowing the linear relationship between low-cloud fraction and lower-tropospheric stability to emerge. If we expand our criteria to more broadly capture low-cloud regimes (by relaxing the constraint on lower-tropospheric stability to include all points with at least one season ≥ 15 K, *cf.*, Figure 2) the distribution of regression slopes broadens, becoming similar to that constructed by sampling the four geographic stratocumulus regions. These results support the idea that the relationship between low-cloud fraction and lower-tropospheric stability, so evident in the seasonal statistics of stratocumulus regions, is likely the signature of the particular dynamics of these regimes.

5. Conclusion

We have used the equilibrium statistics of a mixed-layer model, forced by estimates of varying states at different time scales, to explore the relationship between low-cloud fraction and lower-tropospheric stability in subsidence, or low-cloud, regions in subtropics. Boundary conditions for the model were derived from the 40 year reanalysis of meteorological data by the European Center for Medium Range Weather Forecasts. Notwithstanding a number of simplifying assumptions, many of which can and should be improved upon, the model climatology seems to capture essential aspects of the low-cloud climatology as represented by ISCCP. In particular the positive correlation between low-cloud fraction and lower-tropospheric stability that is so evident in the data also emerges from the equilibrium of the model. When forced over states that capture synoptic variability, *e.g.* forcing time scale less than a week, the relationship becomes most comparable to the data. Sensitivity tests show that among individual meteorological parameters and their variabilities, incorporating daily variations in large-scale divergence improves the behavior of the model most markedly. We believe the behavior of the mixed-layer model improves when the solutions incorporate the full distribution of divergence for two reasons. First, cloud fraction in the model is a strongly non-linear function of divergence. Hence the model cloud fraction depends on representing the full variability in the distribution of divergence for a given value of lower-tropospheric stability, and this receives substantial contributions from variability at short times scales. Second, given this non-linearity, a broad distribution of divergence reduces the sensitivity of the results to biases in the model. Such improvement in representing the relationship is less sensitive to thermodynamic fields because model's response to them is rather linear and their distribution changes less than the factors influencing mass fields as sampling frequency increases.

Further exploration of factors influencing the relationship between the fraction of low clouds and the stability of the lower troposphere suggests that within stratocumulus regimes, *i.e.,* regions of prevailing subsidence with values of lower-tropospheric stability centered near 18 K, such relationships are relatively consistent. However away from such regions the relationships might not be valid. These results suggest that such relationships (correlations) are likely proxies for the statistics of the underlying forcing (or boundary conditions) of the marine boundary layer, and might not be universal when changing dynamic regimes. Fortunately, based on these results, it appears that physically based models that incorporate important elements of mixed layer theory have a good chance of representing the observed empiricism on low-cloud fraction (if suitably forced).

Acknowledgments.

ECMWF ERA-40 data used in this study were obtained from the data systems section at the National Center for Atmospheric Research. The ISCCP D2 data were obtained from the International Satellite Cloud Climatology Project data archives maintained by the Atmospheric Sciences Data Center at NASA Langley Research Center. This research was a part of the Low-Latitude Cloud Feedbacks Climate Process Team, and was partially supported by National Science Foundation, Grant# ATM-0336849. Part of this work was performed under the auspices of the U.S. Department of Energy by Lawrence Livermore National Laboratory under Contract DE-AC52-07NA27344.

APPENDIX

Nondimensional analysis

Equilibrium solutions to the MLM model take the nondimensional form:

$$\frac{h_e}{h_0} = \beta_h - \mu_h \tag{A1}$$

$$\frac{\langle s_l \rangle_e}{s_{l,0}} = 1 + \frac{\beta_s}{1+\beta_h}(\beta_h - (\beta_h - \mu_h)\mu_s - \sigma) \tag{A2}$$

$$\frac{\langle q_t \rangle_e}{q_{t,0}} = 1 + \frac{\beta_q}{1+\beta_h}(\beta_h - (\beta_h - \mu_h)\mu_q) \tag{A3}$$

$$h_0 = V/\mathcal{D} \tag{A4}$$

$$\beta_h = E/V \tag{A5}$$

$$\beta_s = (s_{l,+} - s_{l,0})/s_{l,0} \tag{A6}$$

$$\beta_q = (q_{t,+} - q_{t,0})/q_{t,0} \tag{A7}$$

$$\mu_h = \frac{\langle \tilde{u} \rangle \cdot \nabla h}{V} \tag{A8}$$

$$\mu_s = \frac{\langle \tilde{u} \rangle \cdot \nabla \langle s_l \rangle}{V(s_{l,+} - s_{l,0})/h_0} = \frac{\langle \tilde{u} \rangle \cdot \nabla \langle s_l \rangle}{\mathcal{D}(s_{l,+} - s_{l,0})} \tag{A9}$$

$$\mu_q = \frac{\langle \tilde{u} \rangle \cdot \nabla \langle q_t \rangle}{V(q_{t,+} - q_{t,0})/h_0} = \frac{\langle \tilde{u} \rangle \cdot \nabla \langle q_t \rangle}{\mathcal{D}(q_{t,+} - q_{t,0})} \tag{A10}$$

$$\sigma = \frac{\Delta F_R}{V(s_{l,+} - s_{l,0})} \tag{A11}$$

In the above, h_0 combines the effect from divergence, $\mathcal{D}$, and wind speed, V; β_s represents the normalized stability across the stratocumulus-topped boundary layer (STBL), *i.e.* between surface and just above the STBL, which roughly captures the trend in lower-tropospheric stability or estimated inversion stability (Wood and Bretherton, 2006) in subtropics; β_q is the normalized moisture jump between the free troposphere and surface; μ_h, μ_s and μ_q denote normalized advective terms and σ

stands for the combined effect from V and stability, normalized by the cloud-top radiative cooling, ΔF_R, which we take as almost a constant in this study.

All the nondimensional parameters (A4 – A11) can be expressed in terms of large-scale boundary conditions except β_h represents the entrainment exchange velocity normalized by the surface exchange velocity.

In addition to these parameters, the occurrence probability of insufficient divergence, $\varpi_{\mathcal{D}} = \int_{-\infty}^{\mathcal{D}_c} p(\mathcal{D}) d\mathcal{D}$, likely has a strong influence on the statistics of the equilibria. Although, β_s stands out at the seasonal timescale to correlate with low-cloud fraction most. As observed in Figure 6, 8 and 15, Namibia MAM (March, April and May) and Canary JJA (June, July and August) tend to be outliers with their seasonal means well away from the regression and more independent of β_s locally. Figure 17 shows that in both regions, low-cloud fraction is highly correlated to $\beta_h/(1-\varpi_{\mathcal{D}})$. This suggests in these two regions, low-cloud fraction is affected by the divergence distribution and how we specify the growth rate of the stratocumulus-topped boundary layer. Departures from the observed climatology may thus equally reflect errors in the forcing distribution (especially for Namibia) as much as problem with the model.

REFERENCES

Bretherton, C. S. and M. C. Wyant, 1997: Moisture transport, lower tropospheric stability, and decoupling of cloud-topped boundary layers. *J. Atmos. Sci.*, **54**, 148–167.

Caldwell, P. and C. Bretherton, 2008: Response of a subtropical stratocumulus-capped mixed layer to climate and aerosol changes. *J. Climate*, accepted.

Collins, W. D., P. J. Rasch, and Others, 2004: Description of the NCAR Community Atmosphere Model (CAM 3.0), Technical Report NCAR/TN-464+STR. Tech. rep., National Center for Atmospheric Research, Boulder Colorado. 210pp.

Grenier, H. and C. S. Bretherton, 2001: A moist PBL parameterization for large-scale models and its application to subtropical cloud-topped marine boundary layer. *Mon. Wea. Rev.*, **129**, 357–377.

Klein, S. A., 1997: Synoptic variability of low-cloud properties and meteorological parameters in the subtropical trade wind boundary layer. *J. Climate*, **10**, 2018–2039.

Klein, S. A. and D. L. Hartmann, 1993: The seasonal cycle of low stratiform clouds. *J. Climate*, **6**, 1587–1606.

Klein, S. A., D. L. Hartmann, and J. R. Norris, 1995: On the relationships among low-cloud structure, sea surface temperature, and atmospheric circulation in the summertime northeast Pacific. *J. Climate*, **8**, 1140–1155.

Lewellen, D. C. and W. Lewellen, 1998: Large-eddy boundary layer entrainment. *J. Atmos. Sci.*, **55**, 2645–2665.

Lilly, D. K., 1968: Models of cloud topped mixed layers under a strong inversion. *Quart. J. Roy. Meteor. Soc.*, **94**, 292–309.

Lock, A., 2001: The numerical representation of entrainment in parameterizations of boundary layer turbulent mixing. *Mon. Wea. Rev.*, **129**, 1148–1163.

Medeiros, B. P., A. Hall, and B. Stevens, 2005: What controls the mean depth of the PBL? *J. Climate*, **18**, 3157–3172.

Moeng, C.-H. and B. Stevens, 1999: Marine stratocumulus and its representation in GCMs. *General Circulation Model Development: Past, Present, and Future*, D. A. Randall, Ed., Academic Press, 577–604.

Randall, D. A., J. A. Abeles, and T. G. Corsetti, 1985: Seasonal simulations of the planetary boundary layer and boundary-layer stratocumulus clouds with a general circulation model. *J. Atmos. Sci.*, **42**, 641–676.

Randall, D. A. and M. J. Suarez, 1984: On the dynamics of stratocumulus formation and dissipation. *J. Atmos. Sci.*, **41**, 3052–3057.

Rossow, W. and R. A. Schiffer, 1999: Advances in understanding clouds from ISCCP. *Bull. Amer. Meteor. Soc.*, **80**, 2261–2287.

Schubert, W. H., J. S. Wakefield, E. J. Steiner, and S. K. Cox, 1979: Marine stratocumulus convection. Part II: Horizontally inhomogeneous solutions. *J. Atmos. Sci.*, **36**, 1308–1324.

Siebesma, A. P., et al., 2003: A large eddy simulation intercomparison study of shallow cumulus convection. *J. Atmos. Sci.*, **60**, 1201–1219.

Siems, S. T., D. Lenschow, and C. S. Bretherton, 1993: A numerical study of the interaction between stratocumulus and the air overlying it. *J. Atmos. Sci.*, **50**, 3663–3676.

Slingo, J. M., 1987: The development and verification of a cloud prediction scheme for the ECMWF model. *Quart. J. Roy. Meteor. Soc.*, **113**, 899–927.

Stevens, B., 2000: Cloud transitions and decoupling in shear-free stratocumulus-topped boundary layers. *Geophy. Res. Let.*, **27**, 2557–2560.

Stevens, B., 2002: Entrainment in stratocumulus mixed layers. *Quart. J. Roy. Meteor. Soc.*, **128**, 2663–2690.

Stevens, B., A. Beljaars, S. Bordoni, C. Holloway, M. Köhler, S. Krueger, V. Savic-Jovcic, and Y. Zhang, 2007: On the sturcture of the lower troposphere: July 2001 near 120W and 30N. *Mon. Wea. Rev.*, **135**, 985–1005.

Stevens, B., Y. Zhang, and M. Ghil, 2005: Stochastic effects in the representation of stratocumulus-topped mixed layers. *Proceedings. ECMWF Workshop on Representation of Sub-grid Processes Using Stochastic-Dynamics Models*, Shinfield Park, Reading, UK, ECMWF, pp.79–90.

Stevens, B., et al., 2003a: DYCOMS-II. *Bull. Amer. Meteor. Soc.*, **84**, 579–593.

Stevens, B., et al., 2003b: On entrainment in nocturnal marine stratocumulus. *Quart. J. Roy. Meteor. Soc.*, **129**, 3469–3492.

Suarez, M., A. Arakawa, and D. Randall, 1983: The parameterization of the planetary boundary layer in the UCLA general circulation model: formulation and results. *Mon. Wea. Rev.*, **111**, 2224–2243.

Turton, J. D. and S. Nicholls, 1987: A study of the diurnal variation of stratocumulus using a multiple mixed layer model. *Quart. J. Roy. Meteor. Soc.*, **113**, 969–1009.

Uppala, S. M., et al., 2005: The ERA-40 re-analysis. *Quart. J. Roy. Meteor. Soc.*, **131**, 2961–3012.

Wood, R. and C. S. Bretherton, 2006: On the relationship between stratiform low cloud cover and lower-tropospheric stability. *J. Climate*, **19**, 6425–6432.

Wyant, M. C., C. S. Bretherton, H. A. Rand, and D. E. Stevens, 1997: Numerical simulations and a conceptual model of the stratocumulus to trade cumulus transition. *J. Atmos. Sci.*, **54**, 168–192.

Zhang, Y., B. Stevens, and M. Ghil, 2005: On the diurnal cycle and susceptibility to aerosol concentrations in a stratocumulus-topped mixed layer. *Quart. J. Roy. Meteor. Soc.*, **131**, 1567–1583.

List of Figures

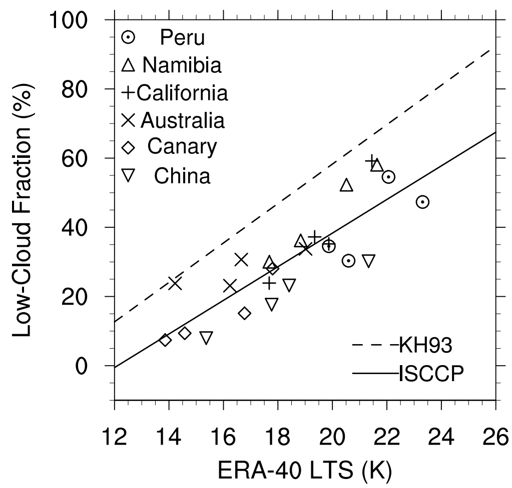

FIG. 1. The least-square regression (solid line) between low-cloud fraction (LCF) from the International Satellite Cloud Climatology Project (ISCCP) and lower-tropospheric stability (LTS) from ECMWF Reanalysis (ERA-40). Different markers denote 12-year (1990-2001) seasonal means in six subtropical regions as shown in Figure 2. The dashed line is the regression between LCF and LTS from Klein and Hartmann (1993).

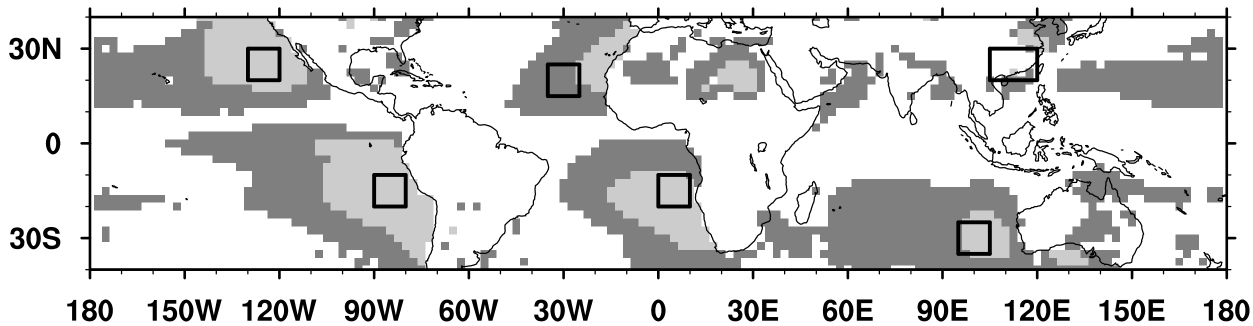

FIG. 2. Boxes show the subtropical stratocumulus regions from Klein and Hartmann (1993): California (20°-30°N, 120°-130°W), Canarian (15°-25°N, 25°-35°W), China (20°-30°N, 105°-120°E), Peruvian (10°-20°S, 80°-90°W), Namibia (10°-20°S, 0°-10°E), and Australia (25°-35°S, 95°-105°E). Shading denotes locations where the climatological (1987-2001) conditions are suggestive of low-cloud conditions in at least one season, based on ECMWF Reanalysis (ERA-40) vertical motion in the mid- and lower-troposphere and the lower-tropospheric stability (LTS). Light shading uses LTS $>$ 18.55 K while dark shading uses LTS $>$ 15 K.

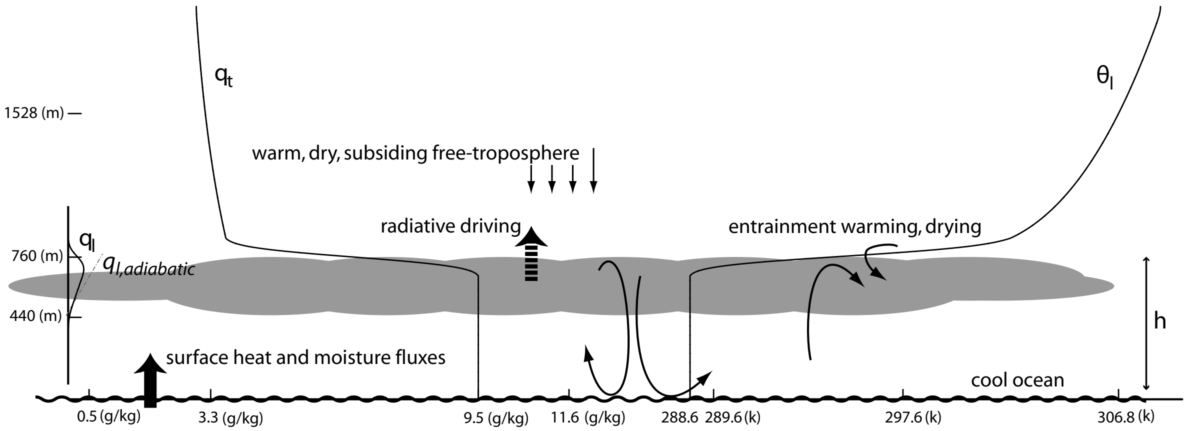

FIG. 3. Well-mixed stratocumulus-topped boundary layer based on the mean state measured by DYCOMS-II, from Stevens et al. (2007).

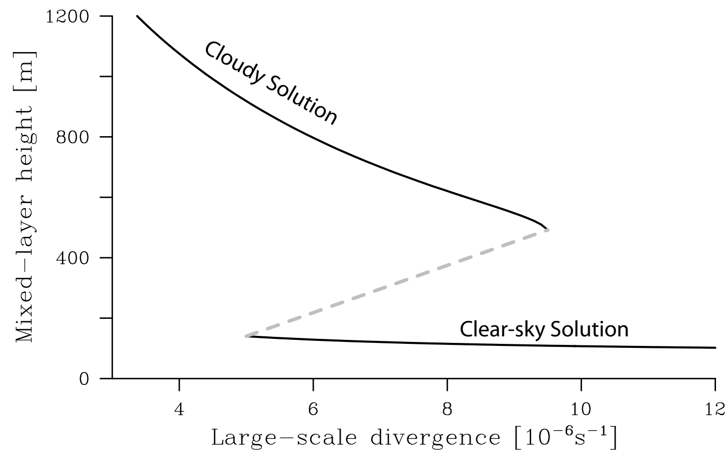

FIG. 4. A conceptual illustration for the MLM's multiple equilibria behavior, after Randall and Suarez (1984). Two solid lines are the stable solutions: cloudy and clear-sky. Dashed line is the unstable solution.

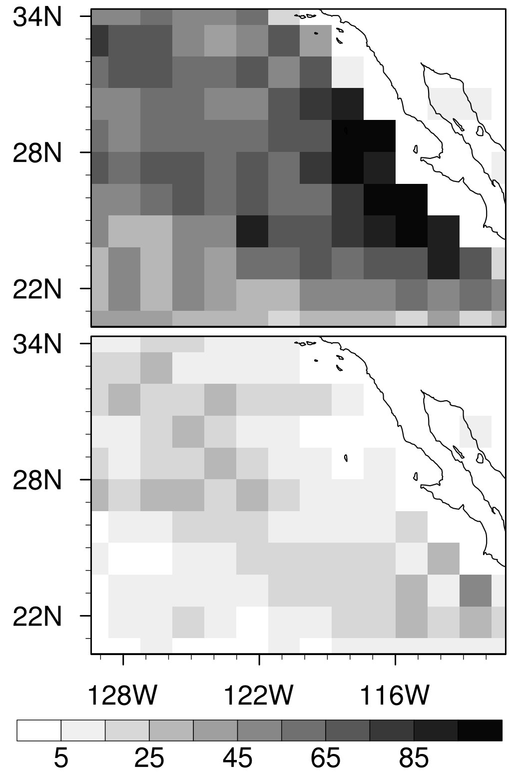

FIG. 5. Low-cloud fraction (in percent) offshore of southern California, July 2001 from MLM equilibrium simulation forced by ERA-40 daily mean data. The top panel shows the results with cloudy initial states while the bottom one shows the difference (decrease) if using clear-sky initial states.

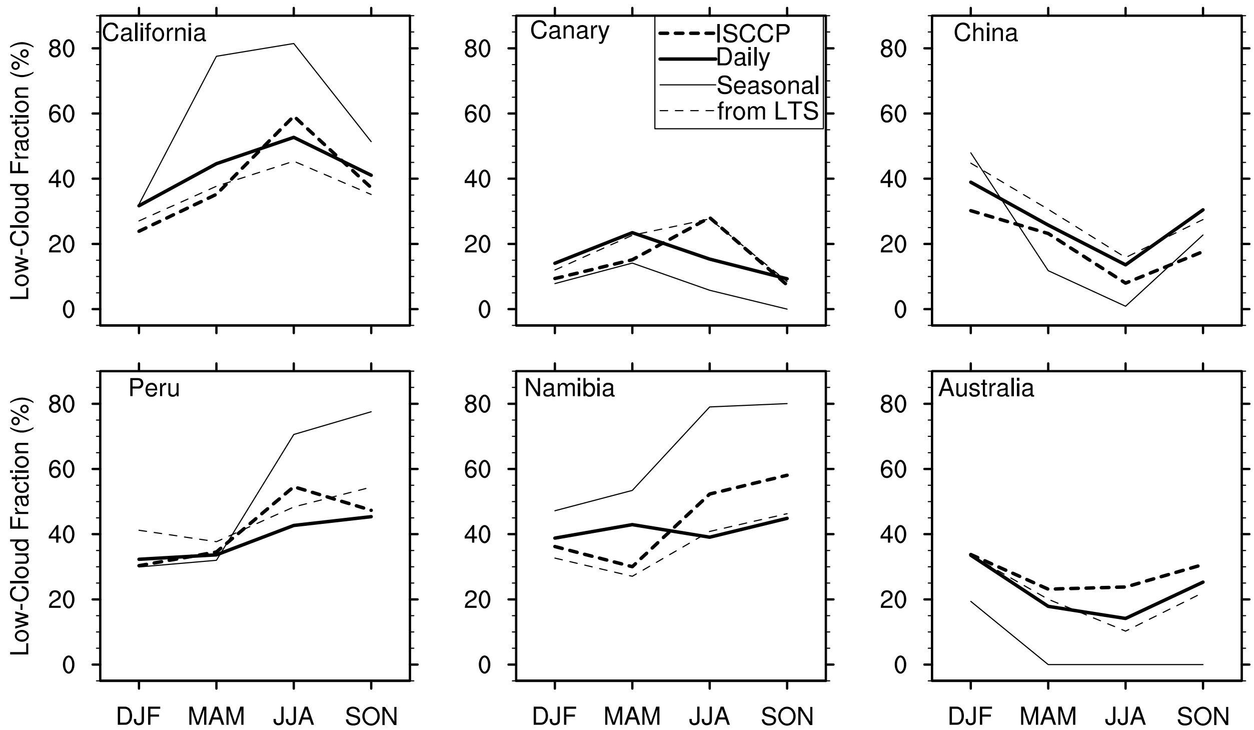

FIG. 6. Seasonal cycles of subtropical low-cloud fraction (LCF) from ISCCP data (dark dashed), MLM daily run (dark solid) and MLM seasonal run (light solid). Light dashed line denotes the LCF diagnosed from lower-tropospheric stability (LTS) based on the regression between ISCCP LCF and ERA-40 LTS in Figure 1.

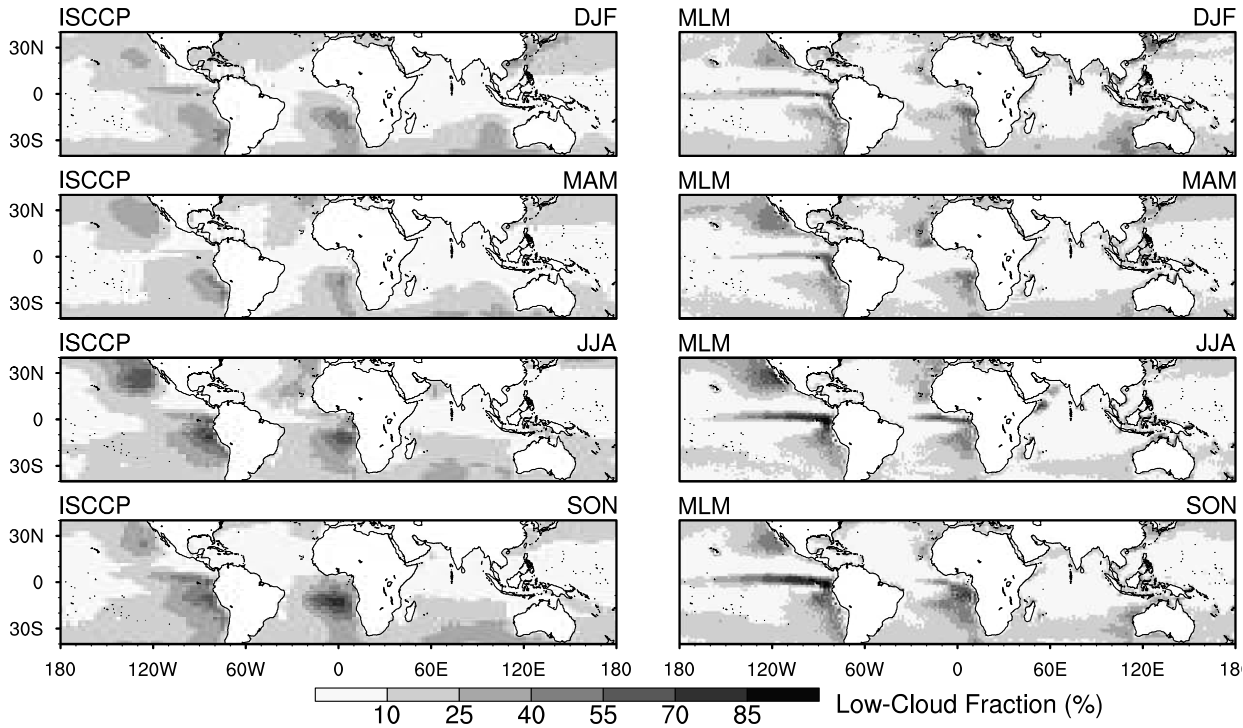

FIG. 7. Seasonal mean low-cloud fraction measured by ISCCP (left) and indicated from the mixed-layer model equilibria with daily forcing (right) over ocean averaged in 12 years (1990-2001).

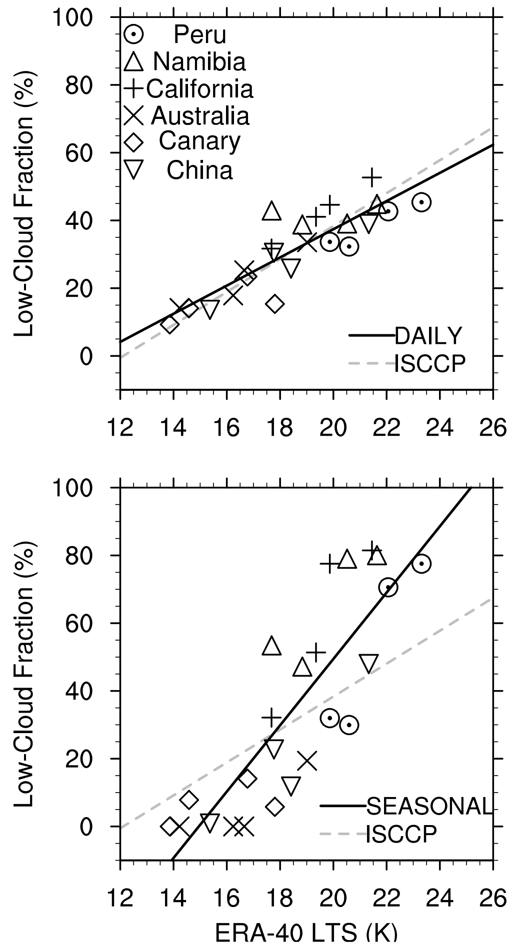

FIG. 8. The least-square regression between seasonal area-mean lower-tropospheric stability (LTS) and low-cloud fraction (LCF) from the MLM equilibria forced by ERA-40 daily data (top) and seasonal averages (bottom). Markers denote different stratocumulus regions in Figure 2. The dashed line is the regression between ISCCP LCF and ERA-40 LTS from Figure 1.

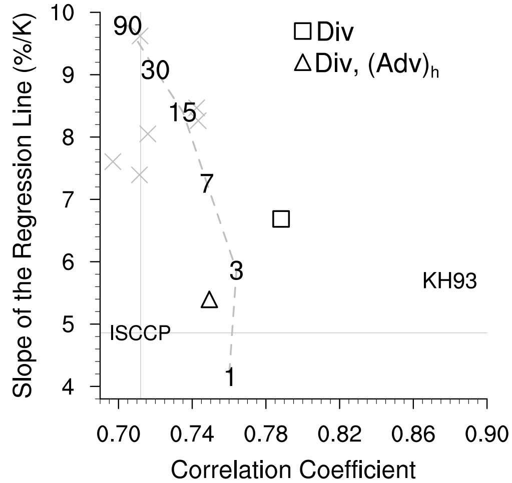

FIG. 9. Transition (gray dashed line) from MLM seasonal (90 days) run to MLM daily (1 day) run in representing the relationship between the MLM equilibrium low-cloud fraction (LCF) and ERA-40 lower-tropospheric stability (LTS): the regression slope (vertical axis) and the correlation coefficient (horizontal axis). Numbers along the dashed line denote the number of days over which daily data is averaged to produce large-scale forcings for the MLM. The gray crosses denote the sensitivity runs in which all the MLM boundary conditions are seasonal averages except one boundary condition, which varies daily; specifically the square denotes the sensitivity run with daily varying divergence; the triangle denotes a similar sensitivity run, but with daily forcing for both divergence and horizontal mass advection. The intersection of the two gray solid lines, denoted by "ISCCP", represents the regression between ISCCP LCF and ERA-40 LTS in Figure 1. "KH93" represents the regression from Klein and Hartmann (1993).

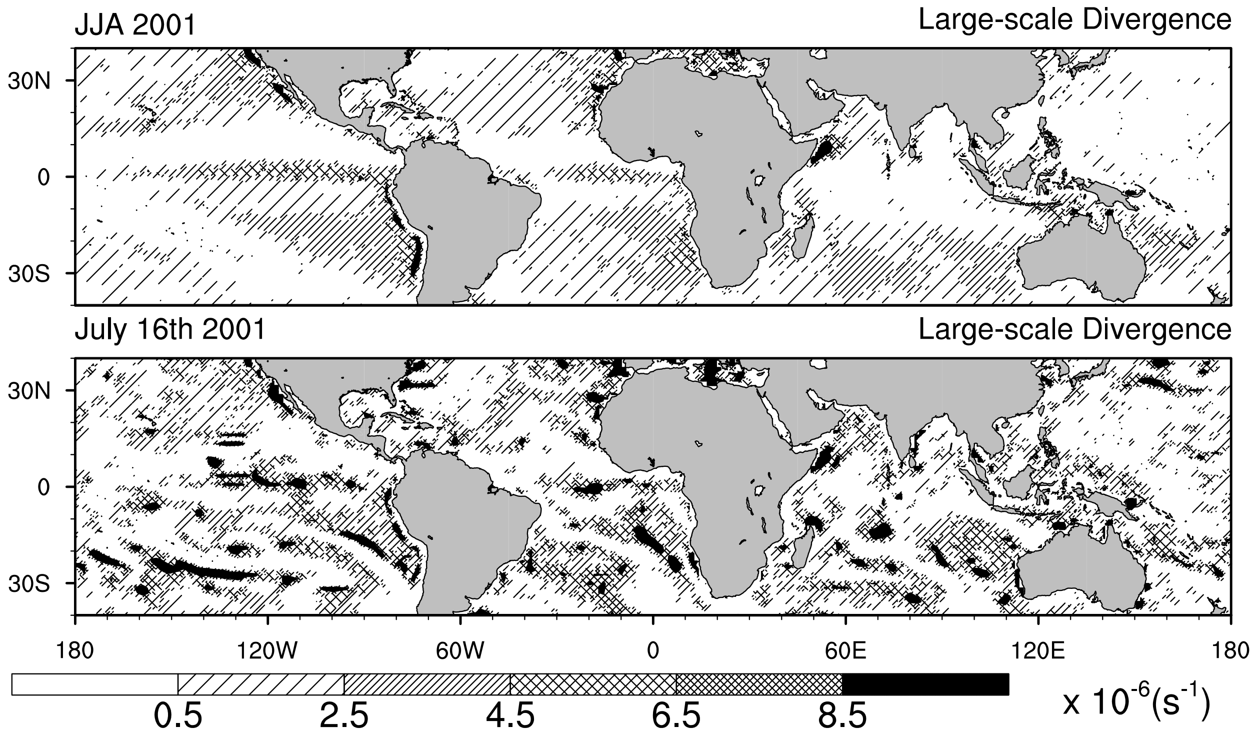

FIG. 10. Large-scale divergence over ocean inferred from ERA-40. Top panel shows the seasonal mean of June, July and August in 2001. Bottom panel shows the daily mean on July 16th, 2001.

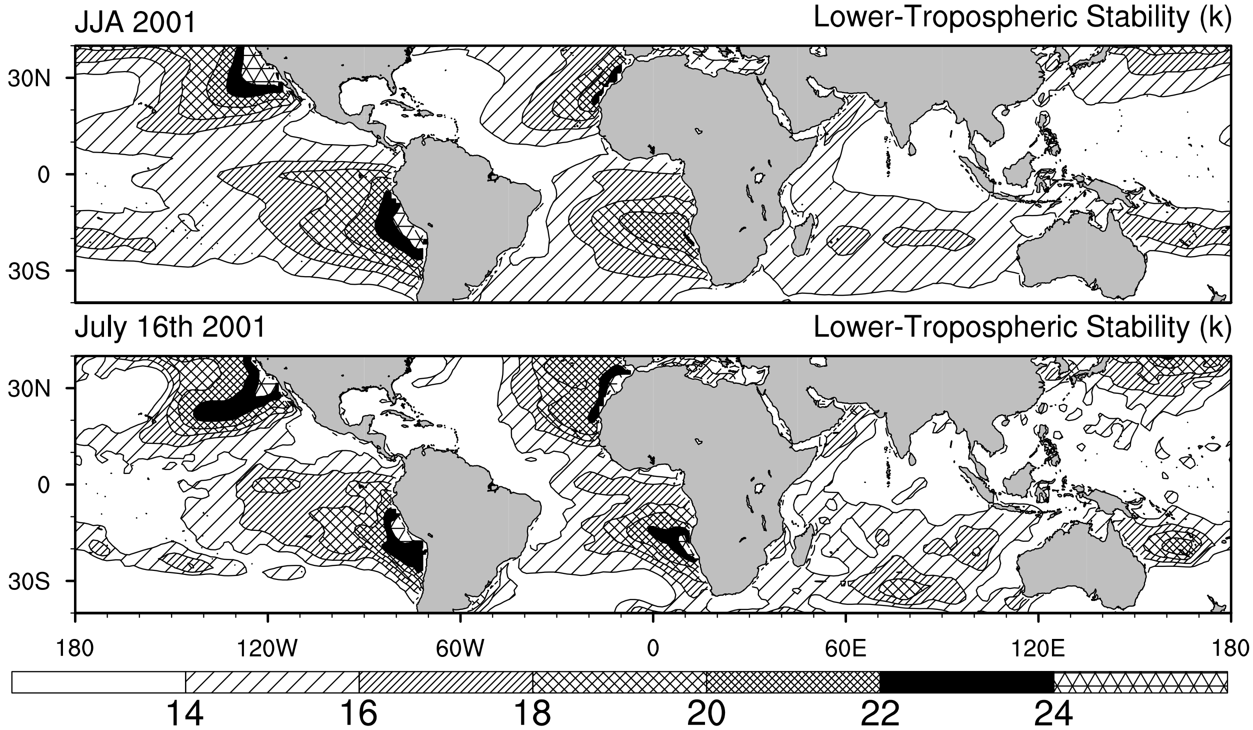

FIG. 11. Same as in Figure 10 but for lower-tropospheric stability over ocean.

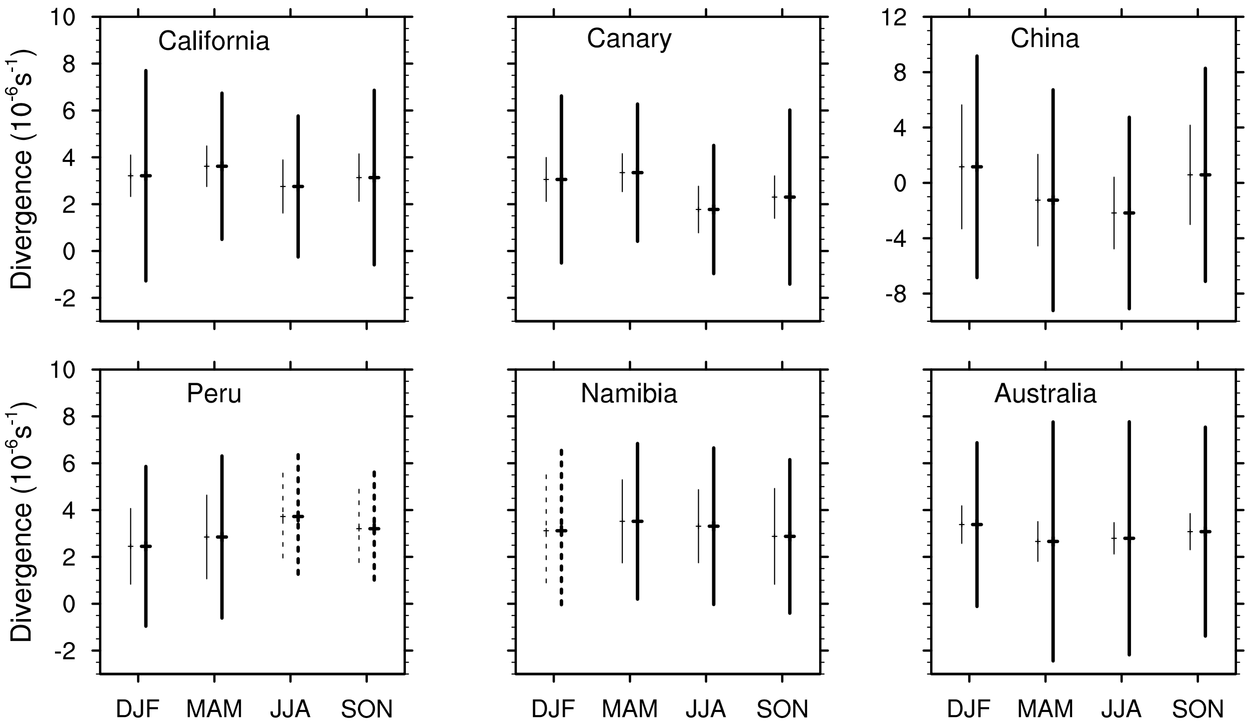

FIG. 12. Short horizontal lines denote long-term seasonal area-mean divergence. Dark (light) vertical spans denote standard deviation (STD) of divergence for daily (seasonal) mean data. Solid (dashed) vertical lines denote seasons in which the STD ratio between seasonal and daily mean data of divergence is less (greater) than the one of lower-tropospheric stability. Notice the Y-Axis for China region is different from others.

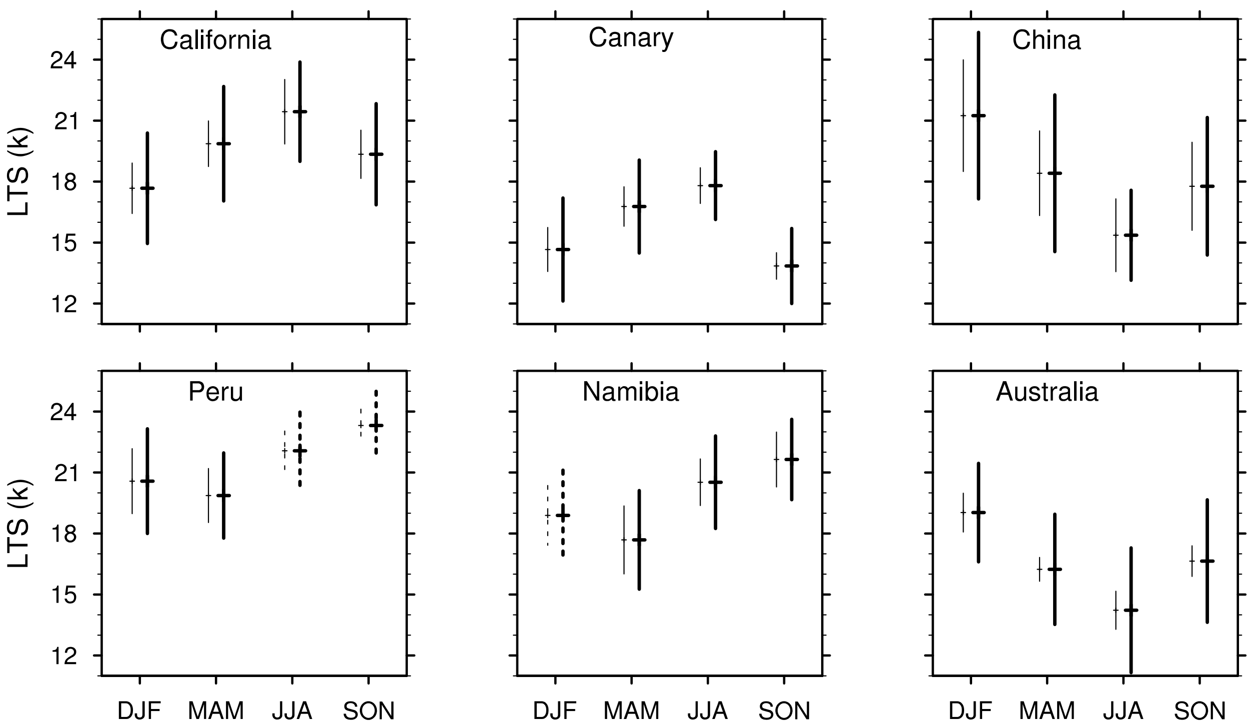

FIG. 13. Same as in Figure 12 but for lower-tropospheric stability.

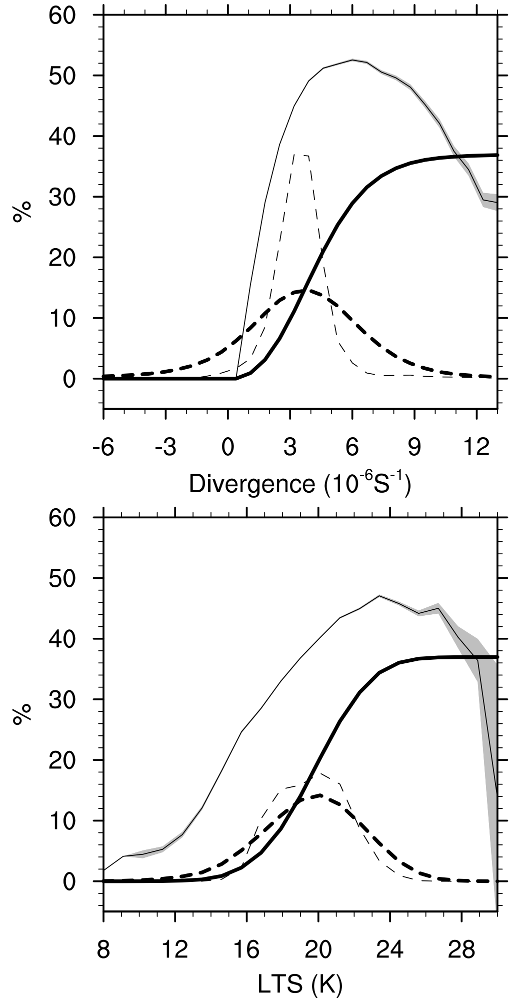

FIG. 14. Statistics for the MLM daily calculations with the seasonal area-mean values satisfying 2.5×10^{-6} s^{-1} $< \mathcal{D} <$ 4×10^{-6} s^{-1} and 16 K <LTS< 22 K. The light solid line shows the cloud fraction conditioned on divergence (top) or lower-tropospheric stability (bottom). The shaded area around the cloud fraction curve shows the standard error. The dashed lines show the probability density function (PDF) of divergence and LTS for daily (dark) and seasonal-averaged (light) data. The dark solid lines are the cumulative cloud fraction integrated from cloud fraction (light solid) upon the PDF for daily data (dark dashed).

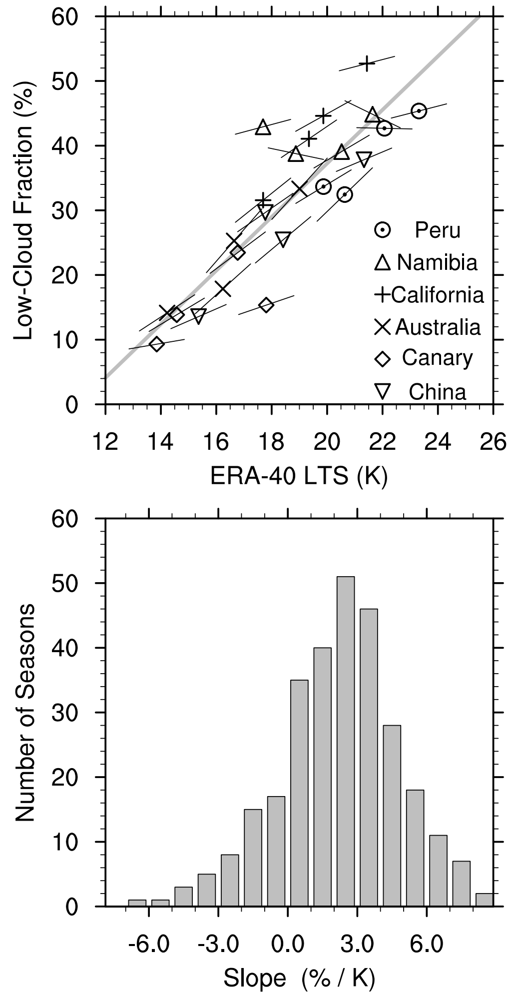

FIG. 15. The emergence of the relationship between low-cloud fraction (LCF) and lower-tropospheric stability (LTS) in different seasons for different regions from the MLM equilibria forced by ERA-40 daily data. Top: The gray line shows the regression between LCF and LTS based on seasonal area-mean values. The black short lines denote the local regression for a particular region and season. Bottom: Histogram of local regression slopes.

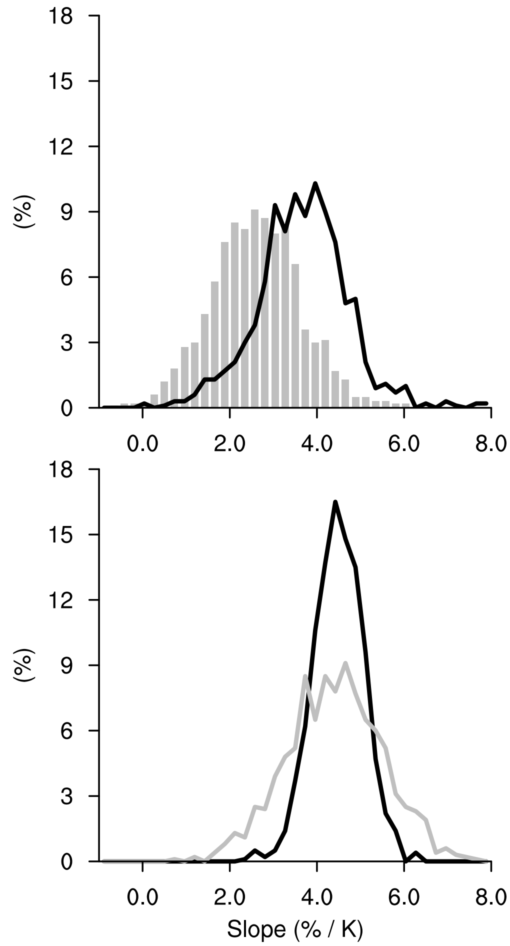

FIG. 16. Top: Distribution of regressions between low-cloud fraction (LCF) and lower-tropospheric stability (LTS) from randomly sampled points from within four of the KH93 stratocumulus regions (Australia, Peru, Californian, Namibian) in Figure 2. Bars show results from the MLM equilibria LCF forced with daily data; the black curve shows the result from sampling the ISCCP data. Four sets of points are drawn from the 12 years within these geographic regions, each set contains approximately the same number of locations as the original regions, producing a set of seasonal averages similar to those in Figure 1 (though without having averaged over multiple years; each seasonal value within the set is drawn from a single year). The bottom panel shows similar distributions based on six sets of points randomly sampled using vertical motion and LTS as selection criteria, LTS > 18.55 K (dark line, corresponds to sampling in the light-shaded region in Figure 2) and LTS > 15 K (light line, corresponds to sampling in the dark-shaded region in Figure 2). All four distributions are based on 1000 regressions, and binned from -1 to 8 % K^{-1} in 40 intervals.

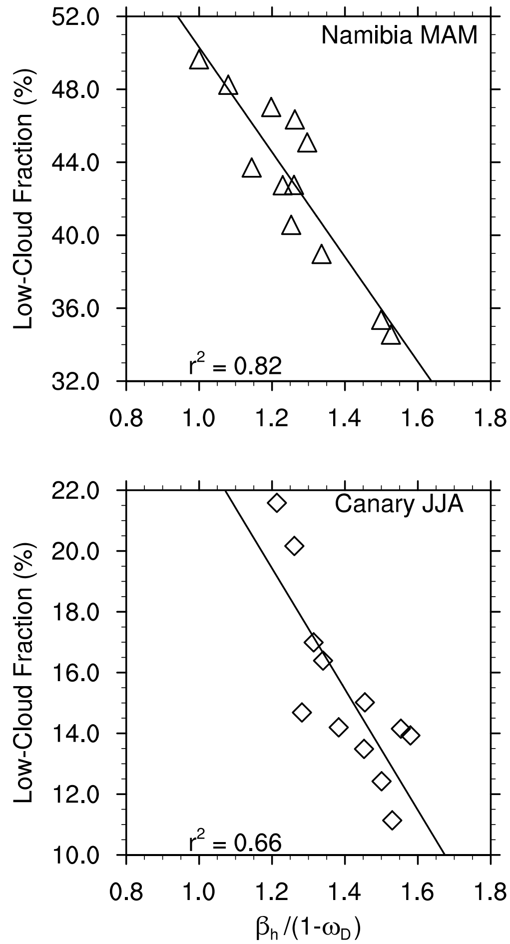

FIG. 17. Least-square regression between low-cloud fraction (LCF) and non-dimensional parameter $\beta_h/(1-\varpi_{\mathcal{D}})$ in the season of March, April and May (MAM) at Namibia (top) and the season of June, July and August (JJA) at Canary (bottom). LCF and $\beta_h/(1-\varpi_{\mathcal{D}})$ are from MLM equilibrium solutions forced by ERA-40 daily mean data in 12 years (1990 to 2001).